Journal of Physics: Conference Series **1561** (2020) 012021 doi:10.1088/1742-6596/1561/1/012021

Prompt gamma imaging in proton therapy - status, challenges and developments

Aleksandra Wrońska for the SiFi-CC group

Marian Smoluchowski Institute of Physics, Jagiellonian University, Łojasiewicza 11, 30-348 Kraków, Poland

URL: http://bragg.if.uj.edu.pl/sificc

E-mail: aleksandra.wronska@uj.edu.pl

Abstract. This paper is an overview of the field of proton therapy monitoring in real time using prompt gamma radiation. Different approaches providing either integrated or differential information are described, and their maturity, limitations and clinical usefulness are discussed. In the second part, the SiFi-CC project is briefly introduced, which aims at the development of a Compton camera for prompt gamma imaging, entirely based on fibres made of a heavy, inorganic scintillator read out by silicon photomultipliers. This compact solution offers very good timing properties, high granularity and a modern data acquisition system, addressing previously identified issues.

1. Introduction

Over seventy years ago Robert Wilson proposed to use ion beams for tumour treatment [1]. He combined the theoretical developments of Hans Bethe describing energy losses of protons and heavier ions when traversing a medium, with the technical achievements of Ernest O. Lawrence, who built the first cyclotron. Although the use of heavier ions allows to enhance biological effectiveness of deposited dose and optimize its conformality, protons still remain the main type of ions used for ion beam radiotherapy, as proposed in Wilson's original paper. The reason for this is simplicity and a relatively low cost of proton cyclotrons compared to the cost of accelerators for heavier ion beams. Thus, proton therapy is one of the most important methods of tumour treatment, next to surgery, chemotherapy, conventional radiotherapy and emerging immunotherapy (Nobel prize in medicine 2018).

The field of proton therapy (PT) was rapidly developing over those seven decades: we learned how to fully utilize the Bragg peak, what are the benefits of fractionated delivery or how to stretch the region of maximum dose (spread-out Bragg peak). In the 1990s there was a transfer of technology from research centres to hospitals. Commercial companies entered the field and around 2000 already the off-the-shelf solutions for PT became available. The XXI century has brought further progress: multi-field irradiation, the use of gantries and scanning pencil beams, modern CT- and PET-assisted evaluation of treatment plans based on sophisticated computer simulations [2]. Those developments were followed by a rapid growth of the number of ion-beam therapy centres, which doubled in the last decade and is close to 100, with another 40 under construction [3].

Proton therapy owes its popularity to the features of proton interaction with matter with its characteristic Bragg peak, which gives a lot of freedom in shaping the distribution of deposited dose and allows to a large extent to spare healthy tissues surrounding the tumour. In particular, the dose depth profile falls down rapidly to zero directly after the Bragg peak, therefore the tissues located deeper do not receive any dose. However, the existence of the Bragg peak and its steep distal falloff in the dose depth profile which are the main advantages of protons over X-rays make the proton therapy more susceptible to errors. The thorough analysis of beam range uncertainties in the patient was performed by Paganetti [4]. The sources of those uncertainties are in patient positioning, patient anatomical changes and translation of CT to water equivalent units. In clinical practice, this leads to the necessity of using safety margins. Each PT centre defines them differently, typical values are from a few millimetres up to over a centimetre for deeply located tumours. They define an extra dose delivered to a patient to account for possible uncontrolled variations of beam range within uncertainties. The way to reduce beam range uncertainties and consequently safety margins would mean a lower dose delivered to a patient and thus lower risk of long-term side effects. This can be achieved by on-line monitoring of the deposited dose distribution in proton therapy. The development of necessary tools was one of the highlights of the 2014 NuPECC report [5].

There are different approaches to ion beam therapy monitoring currently under development. Most of them are based on the same idea of exploiting by-products of patient irradiation with proton beam: acoustic wave [6], protons [7], neutrons [8], β^+-emitters [9] or gamma radiation, which is the main focus of this paper. Of the listed by-products, prompt gamma radiation (PG), typically of a few MeV energy (from 1-2 MeV up to about 7 MeV), has the advantage that it is produced instantaneously and it leaves the patient body mostly without any interaction on its way out. Thus, it carries undisturbed information from the place of its origin. The characteristics of the prompt gamma radiation allows to pinpoint the Bragg peak position and conclude about the deposited dose distribution [10–12]. A variety of different approaches exploiting PG are currently being developed, here they have been divided into two groups. The next section focuses on devices providing one-dimensional information allowing to verify beam range. In the following section the setups enabling full three-dimensional reconstruction of the deposited dose are described, including the SiFi-CC project realized by our group.

2. Proton beam range verification

Range of the proton beam inside the patient can be deduced using different properties of prompt gamma radiation: its spatial, temporal or energy distributions.

2.1. Slit camera

A slit camera is probably the most natural approach, an analogue of a pinhole camera, but providing one-dimensional imaging, see fig. 1. Feasibility studies were performed by several groups [13–15]. The worldwide first test of a slit-camera setup in clinical conditions during patient treatment was reported in ref. [16] by the Dresden group in collaboration with OncoRay and IBA. Their camera was mounted on a movable trolley and consisted of a knife-edge shaped tungsten collimator and an array of 4 mm wide scintillating strips made of LYSO, read out by silicone photomultipliers (SiPMs). The authors focused on the monitoring of inter-fractional range variations rather than absolute range determination and the treatment modality was passively scattered proton therapy. Those variations were determined to be within ± 2 mm. In the following report [17] the group confirmed in the measurements with a head phantom that a precision of ± 2 mm in range verification can be obtained for pencil beam scanning (PBS). However, integration of the setup comprising a massive collimator into the clinical environment still poses a challenge.

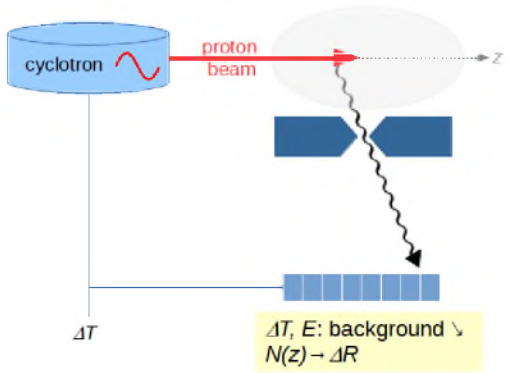

Figure 1. Principle of operation of a slit camera. Prompt gamma rays are imaged using a single slit onto a position-sensitive detector. Spatial hit distribution allows to conclude about range shifts, while time and energy information are used to suppress background.

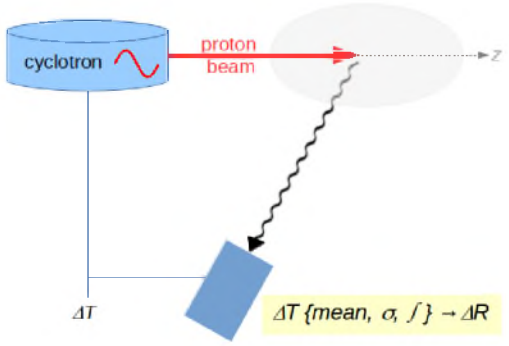

Figure 2. Principle of the PGT and PGPI methods. Both of them rely on recorded distributions of time between beam bunch and registered gamma rays. Analysis of the mean, width and integral of those distributions yields information about beam range.

A generalization of this concept is a multi-slit camera. Smeets *et al.* compared experimentally (using beam energies of 100, 160 and 230 MeV) two collimated setups: one with a knife-edge shaped collimator (KES), and the other with a multi-slit collimator (MPS) of the same weight [18], the slits parallel to each other. The layouts of both collimators were optimized by means of Monte-Carlo simulations. Each collimator was combined with the same detector setup, described in the first paragraph of this section. Due to a smaller field of view, KES provided imaging of the Bragg peak region only, while MPS allowed to image also the beam entrance point. However, in terms of the range retrieval, KES was shown to require only half of the dose MPS needed to obtained the same statistical precision. Thus, the authors concluded KES be the favourable option for further development.

A similar collimated setup was built and tested experimentally by Park *et al.* [19]. The geometry of both the collimator (coarser pattern) and the detector (finer granulation) was somewhat different than in case of [18]. The detector was made of CsI(Tl) and read out by photodiodes, as more radiation-hard than SiPMs. The authors presented reconstructed gamma depth profiles for different beam energies from the range 95−186 MeV, and for each beam energy for four different numbers of delivered protons, between 7.5×10^7 and 7.5×10^9. It turned out possible to locate the distal dose falloff (d90%), defined as the depth of distal 90% dose in a depth-dose curve, within about $2 - 3$ mm of error for the spots which were irradiated with at least 3.8×10^8 protons, regardless of the beam energy. In a typical realistic treatment plan such a dose is delivered only to some of the spots.

A collimated system with many knife-edge shaped slits was studied by Ready *et al.* [20; 21]. In this design the slits formed a 2d pattern, thereby allowing 2d imaging. The gamma quanta were detected using a position-sensitive LFS detector. Experimental tests were performed with a 50 MeV proton beam of clinical beam current, showing the precision of relative Bragg peak localization of about 1 mm (2σ) at the delivery of only 1.8×10^8 protons. A serious limitation, though, was the distance of the collimator front face to the beam axis of only 8 cm. For larger distances the collimator would need to be re-optimized. Measurements with larger proton beam energies are also needed to verify the performance in realistic proton therapy conditions.

2.2. Prompt-gamma timing and peak integrals

Instead of recording the spatial distributions of prompt-gamma radiation, Golnik *et al.* and Testa *et al.* proposed a novel concept of range assessment by prompt-gamma timing (PGT) [22; 23]. The concept was based on the fact, that the time when protons penetrate the patient tissue before stopping depends on the proton range. Only in this time the prompt-gamma photons can be produced. The realization requires a set of two fast detectors providing a good time resolution, one of them registering the moment when proton bunch is about to enter the patient, the other the moment of prompt-gamma detection. Alternatively a signal from cyclotron timing can be used as a start, as depicted in fig. 2. The distribution of time elapsed between the two signals, the so called PGT spectrum, allows to conclude about the proton range by comparing it with the PGT spectrum modelled in the simulations. The simplicity of the setup is an undeniable advantage of this approach.

After initial tests constituting a proof of principle [24], developments towards translation of the method to clinics have been undertaken and reported recently [25]. For this purpose, a series of measurements was performed using a phantom with air cavities and a close-to-realistic treatment plan. The detection unit consisted of a $CeBr_3$ crystal coupled to a classical photomultiplier tube (PMT). The scintillator material was chosen for its short decay time and excellent energy resolution. The signals were fed to and processed in a custom FEE unit U100 attached to the PMT. The signals were analyzed for a single spot or summed up over the whole layer. In the first case there is clearly insufficient statistics and even with additional detection units of the same type it would be hard to reach a precision below 10 mm. However, the PGT spectra for a layer were conclusive and provided a precision of 2-3 mm. The group is planning further development of the setup by adding extra detector units and increasing their rate capacity as well as more tests in the clinical conditions.

In its original form, PGT method uses the statistical momenta of the timing distributions, *i.e.* its mean and width. Krimmer *et al.* proposed to add to those features also peak integrals of the PGT spectra. This variation is called Prompt Gamma Peak Integrals (PGPI). In an experiment with $LaBr_3$ and BaF_2 detectors, a PMMA phantom and a beam of about 65 MeV energy passing through a modulator wheel, the sensitivity of peak integrals to the proton range in the phantom has been demonstrated. The used energy range is a lower limit of that used clinically, a favourable one for PG measurements due to lower count rate and neutron background. Thus the authors used Monte-Carlo methods, benchmarked at that energy, to simulate the setup response at higher energies. A precision of about 3 mm in range verification was obtained. In the multiple-detector setup it is possible to additionally detect target misplacements by comparing signals from different detector units.

2.3. Prompt-gamma spectroscopy

Yet a different approach, so called Prompt Gamma Spectroscopy (PGS) exploiting spectral characteristics of the prompt-gamma radiation, was proposed by Verburg *et al.* [26; 27]. The scheme requires a collimated detector of good energy resolution, directed onto the distal edge of the Bragg peak, as shown schematically in fig. 3. Cross sections of emissions of the PG from discrete transitions, *e.g.* from the reactions $^{12}C(p, p\gamma_{4.44\,MeV})^{12}C$ and $^{16}O(p, p\gamma_{6.13\,MeV})^{16}O$, depend on proton energy in the observed region. Moreover, that dependence is PG energy-specific. Therefore, comparing the yields of the registered prompt gammas corresponding to different discrete transitions, one can conclude about the residual proton energy and thus about the residual range. As a by-product, elemental composition of the observed tissue can be determined. The initial tests were performed in MGH Boston with a single $LaBr_3$ detector with an active anti-Compton shield (ACS) made of BGO, all scintillators read out by classical PMTs. A 15 cm thick lead collimator was used in front of the detector. Timing information (relative to cyclotron timing) and ACS response were used to suppress neutron-induced background. Also

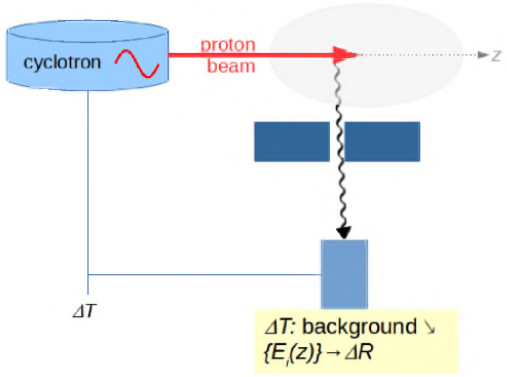

Figure 3. Principle of the PGS method requires registration of PG energy in a collimated detector. Analysis of yields of PGs originating from different discrete transitions provides information about residual range. Time information is used to suppress background.

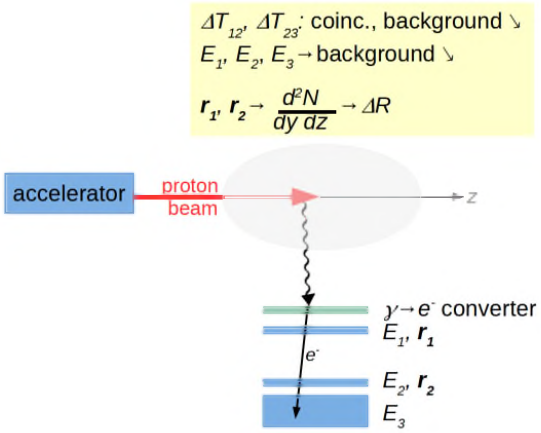

Figure 4. In the GEVI method the PG is first converted into an electron via Compton scattering. The electron is tracked and its energy registered, triple coincidence being a trigger. The tracks, back-projected onto the image plane, deliver a 2d image, which is then projected onto the beam axis, delivering information about beam range. Patterns of energy deposits are used to suppress background from other particle species.

here the counting statistics was of a certain limitation and a summation over a whole layer had to be performed, but as a proof of principle, the experiment was successful. In 2018 the group presented a full-scale clinical prototype consisting of eight $LaBr_3$ detectors, a tungsten collimator and a dedicated custom electronics of high rate capacity ($10^7\,s^{-1}$) [28]. The detectors were mounted on a rotating frame, allowing to adjust the setup to the irradiation direction. Using sophisticated methods of suppression of proton- and neutron induced background as well as Monte-Carlo supported models of the expected detector response, in measurements with a water phantom the authors achieved a 1.1 mm precision in proton range verification at a clinical beam current and dose. The difficulty resulting from limited statistics has been overcome by introducing multiple detection units and a high-throughput front-end electronics. The group is planning commissioning of the system with an anthropomorphic phantom followed by a clinical study with patients.

2.4. Gamma-electron vertex imaging

Although this method is based on prompt-gamma emission, the gamma rays are detected only indirectly via their Compton scattering in a beryllium gamma-electron converter and tracking of the recoiled electron. The concept called GEVI was proposed by a Korean group [29], that recently showed experimental results with test beams [30]. The electron tracking is done with the use of a three-stage hodoscope consisting of two double-sided silicon strip detectors and a calorimeter made of plastic scintillator, as depicted schematically in fig. 4. The electron trajectory is reconstructed based on the hit positions in the silicon detectors and back-projected onto the imaging plane. Event selection by a triple coincidence and cuts on energy deposits in each detection stage allows to suppress background very efficiently. The group performed test experiments with an HDPE phantom and 6.24×10^9 delivered protons for seven beam energies

between 90 and 180 MeV. Two-dmensional images were reconstructed, that were subsequently projected onto the beam axis for the purpose of range determination. The observed distal falloff in the projected images at each energy occurred at 0.94 of the proton range at that energy. According to the authors, the method allows to determine proton range with a precision of 2.7 mm. One should observe, though, that all results were obtained by the group with the same phantom material. For phantoms with other elemental composition (or in case or a real patient treatment) the shape of the distal falloff may be different. Thus, it remains an open question whether the factor 0.94 can be applied and to which extent it is universal. What still needs to be explained is a much lower than expected imaging sensitivity of the system (1.6×10^{-6} *versus* 1.2×10^{-5}), which is probably due to dead time. Nevertheless, the setup, lightweight and simple, is a good candidate for clinical applications.

3. Verification of deposited dose distribution

Even more desirable than the range verification is a full, three-dimensional reconstruction of the deposited dose distribution.

3.1. Positron emission tomography

Although the use of positron emission tomography for proton therapy monitoring is not a prompt-gamma-based method, it must be included in this compilation due to the recent spectacular progress in this field. The method also relies on detection of gamma quanta, even though their energy is lower than in prompt-gamma imaging (511 keV *versus* a-few MeV), see fig. 5. Those annihilation photons are created by positrons released from β^+ emitters produced by the proton beam interacting with the patient tissue. Until recently, PET scans were performed in a different room than the irradiation, or in a different place of the irradiation room, and were considered a useful tool for post-irradiation control rather than a method of proton therapy monitoring *in vivo* and *in situ* [31]. It was believed that the time required to collect sufficient statistics was too large to use that method for this purpose, mostly due to long lifetime of the β^+ emitters reaching up to several minutes. The long acquisition time was leading to biological washout of reaction products which blurred the image. A breakthrough has come with the development of a high-acceptance, high-efficiency INSIDE setup currently operated at CNAO, Pavia [9]. The group of Bisogni built a setup, which contains not only a PET scanner formed by two planar heads, but also a charged particle tracker, which is useful mostly for monitoring of therapy with heavier ion beams. The commissioning showed that the PET scanner operates very well under clinical conditions and allows to reconstruct a map of induced activity of a millimetric resolution. The detector consists of scintillating crystals made of LFS coupled to SiPMs, which in turn are read out by custom electronic modules providing energy and time stamps for the signals. The modules were designed to withstand the rates during irradiation with the synchrotron beams of CNAO. The first clinical test with a patient was reported in 2018 [32]. The on-the-fly reconstructed activity map was quantitatively compared to the simulated map. Comparison was also performed between two consecutive treatment sessions. Range agreement within 1 mm was demonstrated, which proved the method and setup useful for verification of dose distribution in proton therapy. An open question remains, however, whether or not the setup can be integrated with a gantry.

3.2. Prompt-gamma imaging

Another type of setups are used to reconstruct a map of prompt-gamma activity induced in irradiation: Compton cameras (CC). Such detectors consist of two modules: a scatterer and an absorber, as shown in fig. 6. Sometimes setups containing more modules are used to increase detection efficiency. Of interest are the coincident events, in which a signal of Compton-scattered electron is recorded in the scatterer and the scattered gamma is then fully absorbed in the

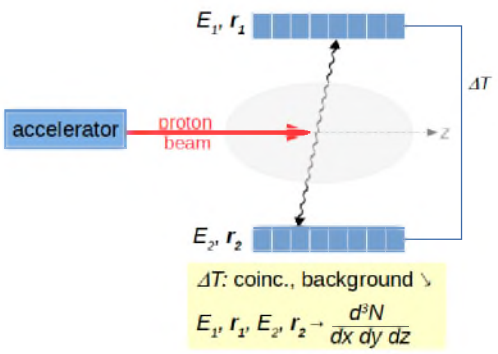

Figure 5. PET used for proton therapy monitoring: lines-of-response built from hit positions allow to reconstruct a three-dimensional map of β^+ activity and compare it with the one expected from Monte-Carlo simulation.

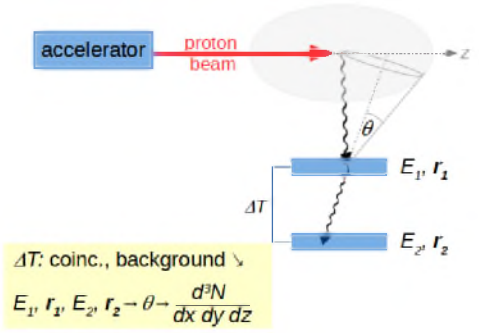

Figure 6. Principle of operation of a Compton camera. From hit positions and energy deposits in the two modules of a CC a cone of possible directions of impinging PGs is reconstructed. Superposition of such cones delivers a three-dimensional map of PG emission.

absorber. Both modules need to provide information on position and deposited energy. Compton kinematics allows to constrain the direction of the original gamma to a surface of a cone or even a part of it, if the scattered electron is tracked. Superposition of many of such cones form an image. Registration of a triple interaction of a gamma in the detector fully determines the energy of the original gamma [33], but on the cost of the reduced detection efficiency. In principle already a single CC is capable of delivering a three-dimensional image, its resolution is rather poor in the direction normal to the modules planes though. A combination of two CCs observing the target at normal directions improves the situation. The prompt-gamma imaging by means of Compton cameras was approached by several groups using different setup designs.

- The Lyon group studied via simulations a CC with a scatterer made of double-sided silicon strip detectors and an absorber consisting of 100 streaked BGO crystals [34]. A similar setup was built in Munich by Thirolf *et al.*, with six planes in the scatterer and a monolithic $LaBr_3$ read out by a multi-anode PMT as an absorber [35]. An image resolution of 3.7 mm was achieved when imaging point-like sources of 1.33 MeV energy. It was also considered to substitute the scatterer with a pixelated GAGG detector developed by the Japanese group (described below) [36].
- A CC of the type semiconductor plus scintillator was also proposed and characterized by the Dresden group [37]. The scatterer consisted of two cross-strip CZT detectors and a single-block LSO detector was used as an absorber. Subsequently the setup was modified and the absorber was replaced with a set of three segmented BGO detectors, each of them read out by a set of 4 classical photomultipliers. That setup was tested with 4.4 MeV gammas and the feasibility of imaging of such energetic gamma quanta was proven [38]. However, the determined setup efficiency and deduced number of expected registered prompt-gamma events were by far insufficient for imaging at clinical dose rates.
- A setup based solely on commercially available, semiconducting CZT detectors was built and tested by the Baltimore group [39]. Those detectors have the advantage of excellent energy resolution, but on the cost of time resolution and longer signal duration than in case of fast scintillators. Polf *et al.* tested extensively the performance of a multi-stage CC. Recently, the group performed measurements with a small-scale prototype under clinical conditions [33] and proved the feasibility of producing 3d images, although it

required sophisticated energy reconstruction and event selection methods. Depending on the irradiation scheme, it was possible to detect range shifts of 2-3 mm.

- A camera consisting of monolithic blocks of $LaBr_3$ scintillator read out by arrays of SiPMs was proposed by Lloså *et al.* [40]. In the initial tests of a first version of the MACACO Compton telescope consisting at that time of two modules, point-like sources of energies 2-7 MeV were reconstructed with 3-5 mm resolution. Although the potential to observe peak-location differences within 10 mm for a 150 MeV beam was demonstrated, available time resolution and detection efficiency still appeared as a problem. The group addressed those issues and reported performance of an improved detector plane [41].
- Another compact (handheld) setup, in which both modules were built from GAGG crystals and SiPMs was proposed by the Japanese group [42]. The modules consisted of small 'pixel' crystals of the dimensions $2 \times 2 \times 4$ mm^3 (scatterer) and of $2 \times 2 \times 2$ mm^3 (absorber). The first setup did not have sufficient resolution to draw conclusions about possible range shifts in proton therapy. The group introduced modifications, among others reducing all pixels to be cubes of 2 mm and substituting SiPMs with multi-anode PMTs, and an attempt to image 4.4 MeV gammas emitted from PMMA phantoms irradiated with a 70 MeV proton beam was undertaken [43]. The conditions were far from clinical - reduced beam current of 3 pA and measurement time of 5 h allowed to collect a vast statistics. Although the capability to use 4.4 MeV prompt gamma rays for imaging was demonstrated, no quantitative analysis of range retrieval or feasibility of use in clinical conditions were presented.

3.3. The SiFi-CC project

SiFi-CC is a yet different design of a Compton camera, proposed by our group [44], *i.e.* physicists from the Jagiellonian University in Cracow, Poland and RWTH Aachen University in Germany. Its name can be resolved as **Si**PM- and scintilation-**Fi**ber-based **C**ompton **C**amera. In the proposed setup both scatterer and absorber will be built of fibers made from an inorganic scintillator of high detection efficiency for a-few MeV gammas. The fibers will be coupled to SiPMs from both sides. Fibers will be arranged into layers and layers will be stacked forming modules. Among the considered materials were GAGG, LuAG and LYSO. Fiber performance was studied experimentally for the geometry of $1 \times 1 \times 100$ mm^3, which is aimed as the CC building blocks [45]. Energy and time resolution, light output and attenuation length for the scintillation light were compared. Those tests allowed to select LYSO, which beside very good performance is rather inexpensive and widely available. Readout will be performed by custom boards developed for the J-PET project [46], which are currently being adapted to feature the ADC functionality necessary for the operation of a CC. The use of high-efficiency materials, large area and good timing properties of LYSO will allow to address issues identified by other groups, such as challenging statistics and background from accidental coincidences. High granularity of the detectors will allow to avoid the problem of pile-ups occurring at high count rates. The fraction of events with pile-ups was estimated for typical clinical conditions by means of Monte-Carlo simulations. Assuming 3×10^8 protons delivered within 10 ms, which are typical for irradiation of a single spot, pile-ups will occur only in $0.5 - 1\%$ of fiber hits, depending on the assumed integration time.

Currently several fronts of development are open. The setup is being optimized by means of Monte-Carlo simulations, which on the fiber level are benchmarked with the results of laboratory tests. Efficiency as well as energy and position resolution are studied for the two considered options of the setup: with all fibers aligned or with crossed planes, as sketched in fig. 7. In both cases the position along the fiber is obtained from the charge ratio of signals from both sides of the fiber, with the expected resolution of 6-10 mm. This can be improved in the clustering algorithm, at least in the crossed-planes option, for the clusters where energy is deposited in two neighbouring layers. In the aligned fiber version the neighbouring layers are shifted by half

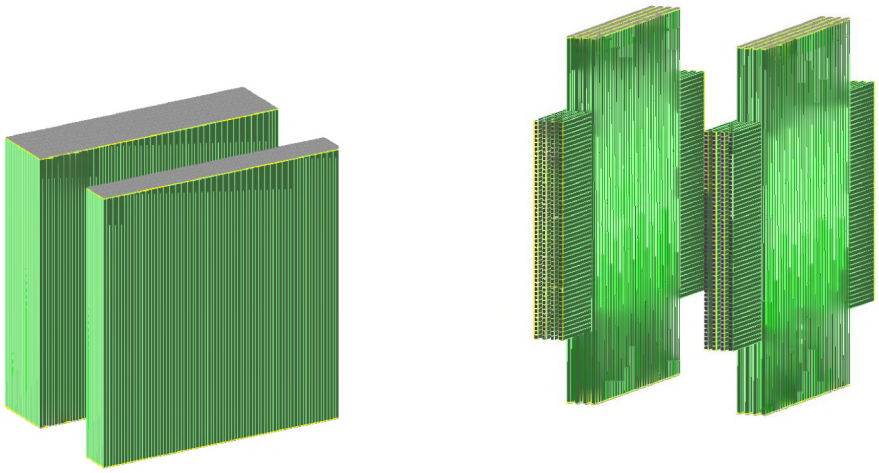

Figure 7. Two studied layouts of the SiFi-CC camera: with all fibers aligned (left), and with crossed layers (right). LYSO fibers are shown in green and SiPMs in gray.

of the fiber size to take advantage of the improved position resolution across the fibers for such events. A software framework for image reconstruction is under development, the LM-MLEM algorithm already implemented. Simulations with realistic position- and energy smearing allow us to expect the point spread function of about 5 mm (FWHM) for a 4.4 MeV source.

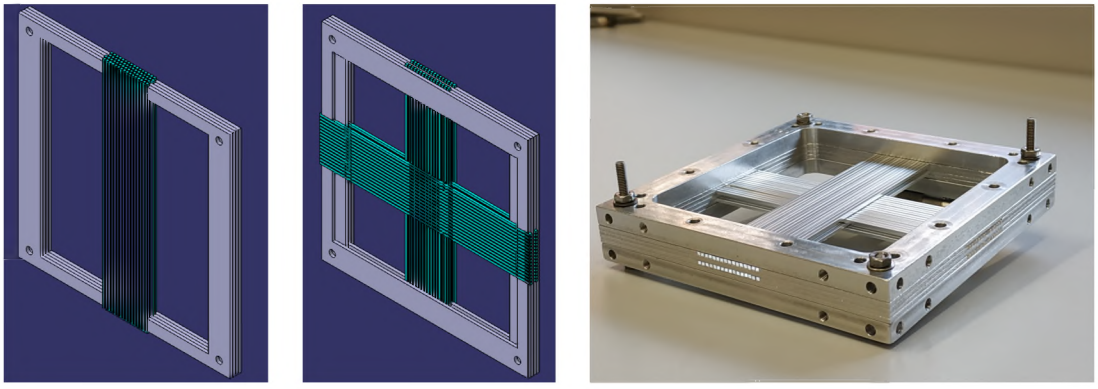

Figure 8. Two schematics of a small-scale prototype of a Compton camera module with different fiber arrangements and a photograph of an existing setup, currently under investigation.

In fact already a single module, when ready, can be used for imaging with a passive collimator. We are planning to test it as a coded-mask setup, combined with a passive collimator with a 2d pattern. However, before constructing the first full-scale module, we are developing a small-scale prototype of four layers, 16 fibers per layer, as shown in fig. 8. The purpose of this is to study the two fiber arrangement options experimentally and validate our simulation as regards cumulative effects of a fiber collection, such as an optical cross-talk *etc.*

4. Summary

Various approaches to on-line monitoring of proton therapy have been presented. Some of them have already been successfully tested clinically with patients. The only commissioned setup to

date providing a three-dimensional verification of the dose is a PET scanner INSIDE. It remains a challenge to construct a 3d imaging device exploiting prompt-gamma radiation which would offer similar performance with a smaller material budget and dimensions.

Acknowledgments
The research is funded under the SONATA BIS grant of the Polish National Science Centre no. 2017/26/E/ST2/00618.

References

[1] Wilson R R 1946 *Radiology* **47** 487–91
[2] Linz U (ed) 2012 *Ion Beam Therapy* (Heidelberg Dordrecht London New York: Springer)
[3] PTCOG web page https://www.ptcog.ch/index.php/facilities-in-operation
[4] Paganetti H 2012 *Physics in Medicine and Biology* **57** R99–R117
[5] NuPECC report 2014: Nuclear Physics for Medicine http://www.nupecc.org/pub/npmed2014.pdf
[6] Parodi K and Assmann W 2015 *Modern Physics Letters A* **30** 1540025
[7] Traini G *et al* 2019 *Physica Medica* **65** 84–93
[8] Marafini M, Gasparini L, Mirabelli R, Pinci D, Patera V, Sciubba A, Spiriti E, Stoppa D, Traini G and Sarti A 2017 *Physics in Medicine and Biology* **62** 3299–312
[9] Bisogni M G *et al* 2016 *Journal of Medical Imaging* **4** 011005
[10] Min C H, Kim C H, Youn M Y and Kim J W 2006 *Applied Physics Letters* **89** 183517
[11] Pinto M *et al* 2015 *Physics in Medicine and Biology* **60** 565–94
[12] Kelleter L *et al* 2017 *Physica Medica* **34** 7–17
[13] Smeets J *et al* 2012 *Physics in Medicine and Biology* **57** 3371–405
[14] Perali I *et al* 2014 *Physics in Medicine and Biology* **59** 5849–71
[15] Cambraia Lopes P *et al* 2015 *Physics in Medicine and Biology* **60** 6063–85
[16] Richter C *et al* 2016 *Radiotherapy and Oncology* **118** 232–7
[17] Nenoff L, Priegnitz M, Janssens G, Petzoldt J, Wohlfahrt P, Trezza A, Smeets J, Pausch G and Richter C 2017 *Radiotherapy and Oncology* **125** 534–40
[18] Smeets J, Roellinghoff F, Janssens G, Perali I, Celani A, Fiorini C, Freud N, Testa E and Prieels D 2016 *Frontiers in Oncology* **6** 156
[19] Park J H, Kim S H, Ku Y, Kim C H, Lee H R, Jeong J H, Lee S B and Shin D H 2019 *Nuclear Engineering and Technology* **51** 1406–16
[20] Ready J, Negut V, Mihailescu L and Vetter K 2016 *Medical Physics* **43** 3717
[21] Ready J F 2016 *Development of a multi-knife-edge slit collimator for prompt gamma ray imaging during proton beam cancer therapy* Phd University of California, Berkeley URL http://adsabs.harvard.edu/abs/2016PhDT.....151R
[22] Golnik C *et al* 2014 *Physics in Medicine and Biology* **59** 5399–422
[23] Testa M, Min C H, Verburg J M, Schümann J, Lu H M and Paganetti H 2014 *Physics in Medicine and Biology* **59** 4181–95
[24] Hueso-González F *et al* 2015 *Physics in Medicine and Biology* **60** 6247–72
[25] Werner T *et al* 2019 *Physics in Medicine and Biology* **64** 105023
[26] Verburg J M, Riley K, Bortfeld T and Seco J 2013 *Physics in Medicine and Biology* **58** L37–L49

[27] Verburg J M and Seco J 2014 *Physics in Medicine and Biology* **59** 7089–106

[28] Hueso-González F, Rabe M, Ruggieri T, Bortfeld T and Verburg J M 2018 *Physics in Medicine and Biology* **63** 185019

[29] Kim C H, Park J H, Seo H and Lee H R 2012 *Medical Physics* **39** 1001–5

[30] Kim C H, Lee H R, Kim S H, Park J H, Cho S and Jung W G 2018 *Applied Physics Letters* **113** 114101–5

[31] Parodi K 2015 *Medical Physics* **42** 7153–68

[32] Ferrero V *et al* 2018 *Scientific Reports* **8** 4100

[33] Draeger E, Mackin D, Peterson S, Chen H, Avery S, Beddar S and Polf J C 2018 *Physics in Medicine and Biology* **63** 035019

[34] Krimmer J *et al* 2015 *Nuclear Instruments and Methods in Physics Research Section A: Accelerators, Spectrometers, Detectors and Associated Equipment* **787** 98–101

[35] Aldawood S *et al* 2017 *Radiation Physics and Chemistry* **140** 190–7

[36] Liprandi S *et al* 2017 Characterization of a Compton camera setup with monolithic LaBr3(Ce) absorber and segmented GAGG scatter detectors *Proceedings of 2017 IEEE Nuclear Science Symposium and Medical Imaging Conference (NSS/MIC)* (IEEE) ISBN 978-1-5386-2282-7

[37] Hueso-González F *et al* 2014 *Journal of Instrumentation* **9** P05002

[38] Golnik C *et al* 2016 *Journal of Instrumentation* **11** P06009

[39] Polf J C, Avery S, Mackin D S and Beddar S 2015 *Physics in Medicine and Biology* **60** 7085–99

[40] Llosá G *et al* 2013 *Nuclear Instruments and Methods in Physics Research, Section A: Accelerators, Spectrometers, Detectors and Associated Equipment* **718** 130–3

[41] Barrio J, Etxebeste A, Granado L, Muñoz E, Oliver J F, Ros A, Roser J, Solaz C and Llosá G 2018 *Nuclear Instruments and Methods in Physics Research, Section A: Accelerators, Spectrometers, Detectors and Associated Equipment* **912** 48–52

[42] Taya T, Kataoka J, Kishimoto A, Iwamoto Y, Koide A, Nishio T, Kabuki S and Inaniwa T 2016 *Nuclear Instruments and Methods in Physics Research Section A: Accelerators, Spectrometers, Detectors and Associated Equipment* **831** 355–61

[43] Koide A *et al* 2018 *Scientific Reports* **8** 8116

[44] Wrońska A, Hetzel R, Kasper J, Lalik R, Magiera A, Rusiecka K and Stahl A 2020 *Acta Physica Polonica B* **51** 17–25

[45] Rusiecka K, Kasper J, Magiera A, Stahl A and Wrońska A 2019 Investigation of the Properties of the Heavy Scintillating Fibers for Their Potential Use in Hadron Therapy Monitoring *Engineering of Scintillation Materials and Radiation Technologies, Selected Articles of ISMART2018* ed Korzhik M and Gektin A (Springer) pp 195–210 ISBN 9783030219703

[46] Niedźwiecki S *et al* 2017 *Acta Physica Polonica B* **48** 1567–76